A two-tiered mechanism of EGFR inhibition by RALT/MIG6 via kinase suppression and receptor degradation

Yuri Frosi,[1] Sergio Anastasi,[1] Costanza Ballarò,[2] Giulia Varsano,[1] Loriana Castellani,[2,3] Elena Maspero,[4] Simona Polo,[4,5] Stefano Alemà,[2] and Oreste Segatto[1]

[1]Istituto Regina Elena, Rome 00158, Italy
[2]Istituto di Biologia Cellulare, CNR, Monterotondo 00016, Italy
[3]Dipartimento di Scienze Motorie e della Salute, Università di Cassino, Cassino 03043, Italy
[4]Istituto IFOM, Fondazione Istituto FIRC di Oncologia Molecolare, Milano 20139, Italy
[5]Dipartimento di Medicina, Chirurgia ed Odontoiatria, Università degli Studi di Milano, Milano 20142, Italy

Signaling by epidermal growth factor receptor (EGFR) must be controlled tightly because aberrant EGFR activity may cause cell transformation. Receptor-associated late transducer (RALT) is a feedback inhibitor of EGFR whose genetic ablation in the mouse causes phenotypes due to EGFR-driven excess cell proliferation. RALT inhibits EGFR catalytic activation by docking onto EGFR kinase domain. We report here an additional mechanism of EGFR suppression mediated by RALT, demonstrating that RALT-bound EGF receptors undergo endocytosis and eventual degradation into lysosomes. Moreover, RALT rescues the endocytic deficit of EGFR mutants unable to undergo either endocytosis (Dc214) or degradation (Y1045F) and mediates endocytosis via a domain distinct from that responsible for EGFR catalytic suppression. Consistent with providing a scaffolding function for endocytic proteins, RALT drives EGFR endocytosis by binding to AP-2 and Intersectins. These data suggest a model in which binding of RALT to EGFR integrates suppression of EGFR kinase with receptor endocytosis and degradation, leading to durable repression of EGFR signaling.

Introduction

The EGF receptor (EGFR) is a receptor tyrosine kinase that instructs key cellular programs such as proliferation, survival, and locomotion. The implementation of these programs requires EGFR signals to be of defined strength within precise boundaries of space and time. While spurious EGFR activation is to be avoided, preventing excess EGFR activity is also crucial because the latter disrupts tissue homeostasis and may lead to cell transformation (Sibilia et al., 2007).

Inadvertent activation of EGFR is prevented by self-inhibitory constraints imposed on both the extracellular ligand-binding region (Burgess et al., 2003) and the intracellular catalytic domain of the receptor (Zhang et al., 2006). Ligand binding relieves these constraints by driving dimerization of EGFR extracellular domains (Burgess et al., 2003). This is conducive to the formation of asymmetric dimers between juxtaposed kinase domains, allowing for allosteric activation of the kinase, receptor auto-phosphorylation, and initiation of downstream signaling (X. Zhang et al., 2007). EGFR signaling is in turn subject to the close control of negative regulatory circuits. Among these, a prominent role is played by (a) receptor endocytosis, which leads to fast internalization of ligand–EGFR complexes (Sorkin and Goh, 2009); and (b) a network of inducible inhibitors that target several pathway components, including the EGFR itself, in order to ensure tight control of EGFR

S. Anastasi, C. Ballarò, and G. Varsano contributed equally to this paper.

Correspondence to Oreste Segatto: segatto@ifo.it

G. Varsano's present address is Unit of Genome Biology, EMBL, Heidelberg 69117, Germany.

Abbreviations used in this paper: CCP, clathrin-coated pit; CHC, clathrin heavy chain; CME, clathrin mediated endocytosis; EBR, ErbB binding region; EGFR, epidermal growth factor receptor; KD, knock-down; MVB, multivesicular body; RALT, receptor-associated late transducer; RED, RALT endocytic domain.

The Rockefeller University Press $30.00
J. Cell Biol. Vol. 189 No. 3 557–571
www.jcb.org/cgi/doi/10.1083/jcb.201002032

signaling over timescales of several hours (Amit et al., 2007; Fry et al., 2009).

RALT (receptor-associated late transducer; also known as MIG6 and ERRFI1) is a transcriptionally induced feedback inhibitor of EGFR (Anastasi et al., 2005; Xu et al., 2005). Increased RALT dosage suppresses EGFR signaling in in vitro cell-based assays (Hackel et al., 2001; Anastasi et al., 2003; Xu et al., 2005) and in mouse tissues such as skin and myocardium (Ballarò et al., 2005; Cai et al., 2009). Silencing of RALT in cultured cells enhances cellular responses induced by EGFR activation (Anastasi et al., 2005; Reschke et al., 2009). Moreover, *Errfi1*$^{-/-}$ mice display a fully penetrant skin phenotype, showing increased thickness of the epidermis, altered cellular differentiation, and enhanced susceptibility to cancerogenesis due to excess EGFR activity and attendant hyper-proliferation of keratinocytes (Ferby et al., 2006).

An important question concerns the identification of the molecular mechanism(s) through which RALT exerts its essential role of EGFR inhibitor and putative tumor suppressor function (Anastasi et al., 2005; Ferby et al., 2006; Y.W. Zhang et al., 2007). Previous studies have demonstrated that RALT inhibits EGFR catalytic activation by binding to ligand-engaged EGFRs via its ErbB binding region (EBR; Xu et al., 2005; Anastasi et al., 2007). In detail, RALT binds to the dimer interface located in the distal portion of the C-terminal lobe of the EGFR kinase domain, thus precluding formation of asymmetric kinase dimers and locking the EGFR kinase in a catalytically unproductive configuration (X. Zhang et al., 2007).

Earlier work had also shown that cytoplasmic RALT relocalizes to internalized EGFR (Anastasi et al., 2003). This creates a conundrum because sustained catalytic activation of the EGFR is held as a *sine qua non* for its ligand-dependent endocytic traffic (Sorkin and Goh, 2009). For example, sorting of ligand-activated EGFR into clathrin-coated pits (CCPs) requires binding of GRB2 to auto-phosphorylated EGFR (Jiang et al., 2003; Huang and Sorkin, 2005; Johannessen et al., 2006) and is prevented by pharmacological inhibition of the EGFR kinase (Sorkina et al., 2002). Catalytic activation of EGFR is also necessary for EGFR–CBL complex formation and CBL-dependent ubiquitylation of EGFR (Levkowitz et al., 1998, 1999). Ubiquitylation plays an obligatory role in routing internalized EGFR molecules into multivesicular bodies (MVBs), a step that terminates EGFR signaling and targets the receptor for destruction into lysosomes (Sorkin and Goh, 2009). Thus, through the kinase-dependent regulation of its own phosphorylation and ubiquitylation, activated EGFR nucleates protein–protein interactions capable of promoting its endocytic traffic from the plasma membrane to late endosomes.

Herein, we address whether RALT-bound EGFR molecules are capable of undergoing endocytosis. We find that RALT is capable of driving the internalization and eventual degradation of EGFR molecules that are neither tyrosine phosphorylated nor ubiquitylated. We ascribe the pro-endocytic activity of RALT to its ability of scaffolding endocytic proteins and propose that RALT ensures durable attenuation of EGFR signaling by integrating two mechanisms so far considered to be mutually exclusive, namely suppression of EGFR catalytic activity and receptor down-regulation.

Results

RALT-bound EGFR undergoes efficient endocytosis

We engineered stable NR6-EGFR cells in which ectopic RALT inhibited EGFR kinase activity by >90% and mimicked the pharmacological suppression of EGFR kinase activity observed in control NR6-EGFR cells upon treatment with the EGFR-specific inhibitor AG1478 (Fig. 1 A). This cellular model is therefore suitable for quantitative biochemical studies of EGFR endocytosis under two different conditions of virtually complete suppression of EGFR catalytic activity.

Cell imaging studies indicated that AG1478 ablated ligand-dependent EGFR internalization in NR6-EGFR cells. In contrast, a rapid relocalization of EGFR to intracellular vesicles was observed in EGF-treated NR6-EGFR/RALT cells, irrespective of AG1478 (Fig. S1 A). Initial rates of [^{125}I]-EGF uptake were comparable in NR6-EGFR/RALT and control cells (Fig. 1 B), with internalization rate constants (K_e; see Materials and methods) being 0.184 ± 0.023 and 0.189 ± 0.029, respectively. In contrast, AG1478 led to a dramatic reduction of [^{125}I]-EGF uptake in NR6-EGFR cells, as reported previously (Sorkina et al., 2002; Fig. 1 B). EGF-driven endocytosis caused extensive down-regulation (Fig. 1 C) and eventual degradation (Fig. 1 D) of EGFR in both control and NR6-EGFR/RALT cells. This was not observed in NR6-EGFR cells treated with the EGF + AG1478 combination (Fig. 1 C; Fig. S1 B). Finally, EGFR and RALT colocalized in vesicular structures labeled by the early (EEA1) and late (LAMP1) endosome markers (Fig. 1 E), indicating that the endocytic traffic of EGFR in NR6-EGFR/RALT cells was associated to sustained EGFR–RALT physical interaction and uninterrupted suppression of EGFR catalytic function.

RALT rescues the endocytic deficit of EGFR Dc214

How can RALT-bound EGFR molecules undergo efficient endocytosis and degradation despite being catalytically inert? We reasoned that RALT itself could form a platform for molecular interactions capable of organizing EGFR endocytic traffic. To test this hypothesis we focused on EGFR Dc214, a catalytically competent EGFR mutant that lacks the C-tail and is therefore unable to couple to canonical EGFR endocytic pathways (Chen et al., 1989). EGFR Dc214 retains RALT binding (Anastasi et al., 2003, 2007) and underwent ligand-dependent endocytosis in serum-starved cells expressing ectopic RALT, but not in control NR6-EGFR Dc214 fibroblasts (Fig. 2 A). Colocalization studies indicated that internalized EGFR Dc214 was routed to early endosomes in complex with RALT (Fig. 2 B). We next addressed whether endogenous levels of RALT protein were sufficient to signal endocytosis of EGFR Dc214. To this end, NR6-EGFR Dc214 cells were rendered quiescent by serum deprivation and subsequently stimulated with 10% serum for 3 h to induce robust expression of RALT protein (Fig. 2, C and D; see also Fiorentino et al., 2000). After serum wash-out, cells were challenged with EGF for 10 min at 37°C. Serum stimulation alone did not induce EGFR Dc214 endocytosis, which was

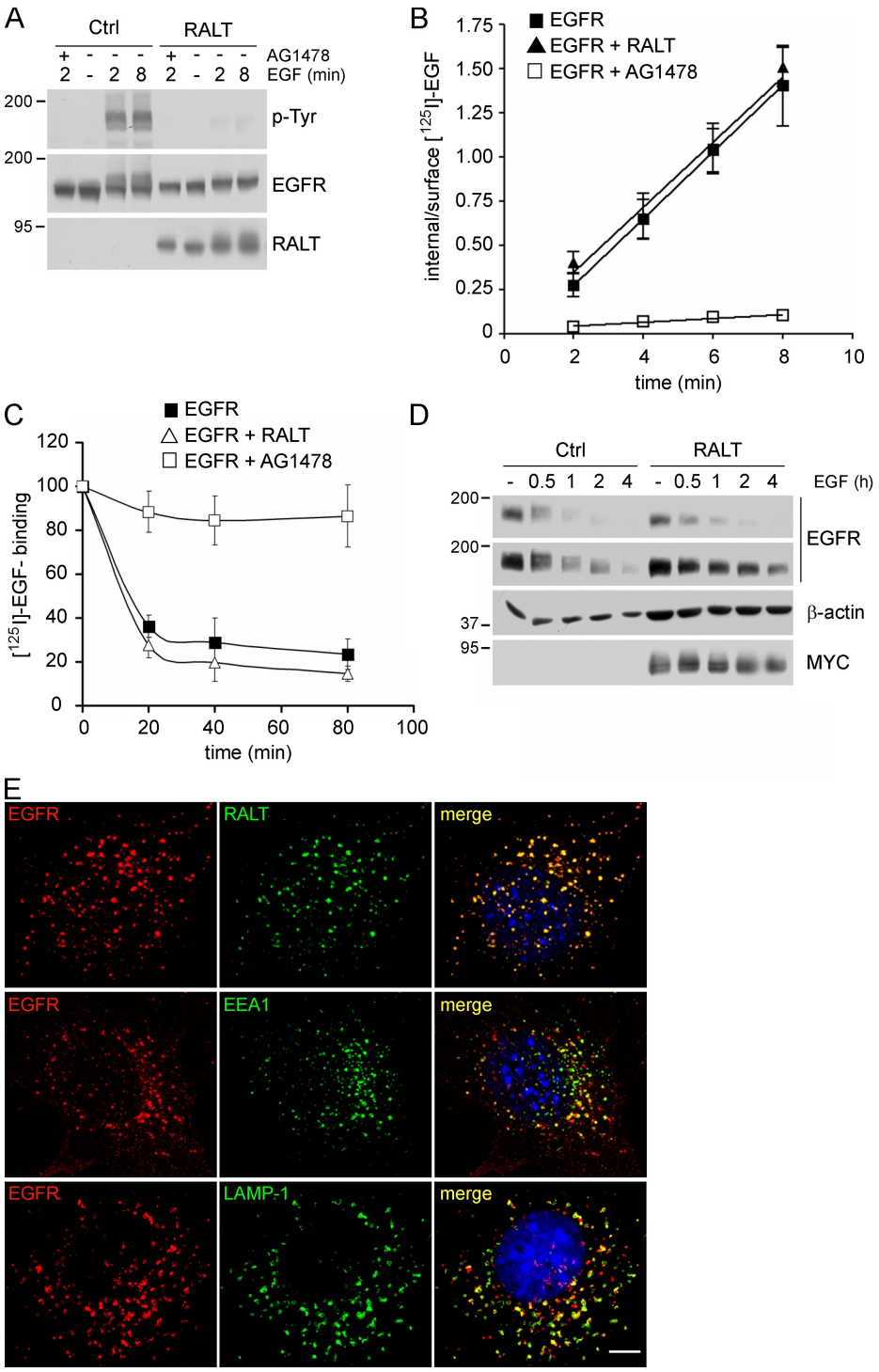

Figure 1. **Kinase inhibition by RALT, but not by AG1478, is associated to normal rates of EGFR endocytosis and down-regulation.** (A) Expression of EGFR and MYC-RALT was reconstituted in NR6 fibroblasts, which lack endogenous EGFR expression. Control and RALT-overexpressing NR6-EGFR cells were rendered quiescent and then stimulated with 100 ng/ml EGF (±3 μM AG1478) for the indicated time. Lysates were immunoblotted as indicated. (B) Control (±3 μM AG1478) and MYC-RALT–expressing NR6-EGFR cells were assayed for [^{125}I]-EGF uptake (1 ng/ml at 37°C for the indicated time). The graph reports the average results ± SD from four independent experiments. (C) Control (±3 μM AG1478) and MYC-RALT–expressing NR6-EGFR cells were made quiescent, incubated at 37°C with 100 ng/ml EGF for the indicated time, and processed to determine residual [^{125}I]-EGF binding at the cell surface (percentage of binding at time 0). Results were averaged from three independent experiments ± SD. (D) EGFR degradation. Control and MYC-RALT–expressing NR6-EGFR cells were rendered quiescent and then stimulated with 100 ng/ml EGF for the indicated time (hours). Lysates were immunoblotted with the indicated antibodies. Two different exposures of the same anti-EGFR autoradiograph are shown. (E) Quiescent MYC-RALT–expressing NR6-EGFR cells were incubated with 20 ng/ml EGF on ice for 30 min. After EGF wash-out, cells were chased at 37°C in EGF-free medium for either 10 min (for EGFR/EEA1 and EGFR/RALT colocalization) or 30 min (for EGFR/LAMP-1 colocalization). Nuclei were stained with Hoechst 33258 (blue). Bar, 5 μm.

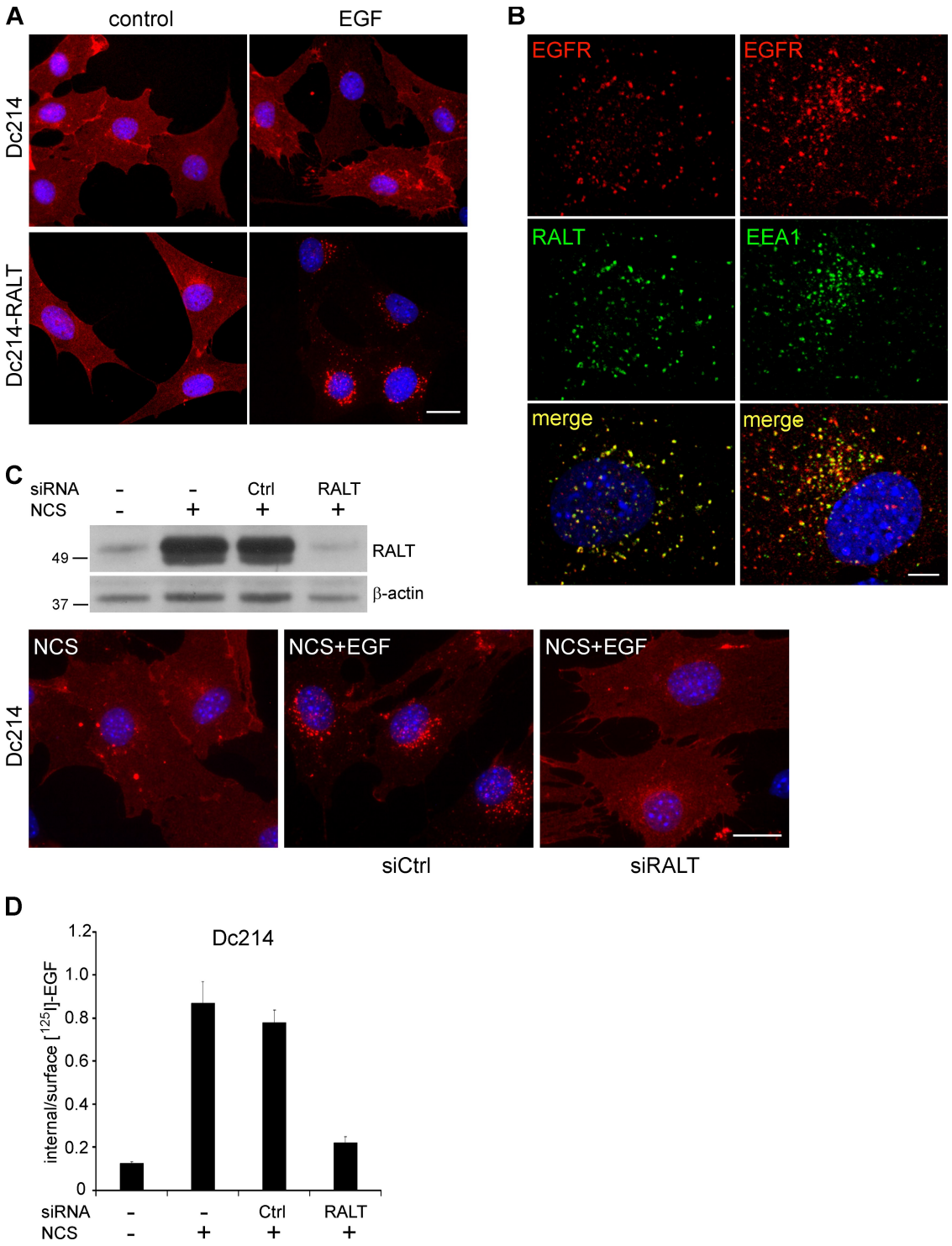

Figure 2. **RALT rescues the endocytic deficit of EGFR Dc214.** (A) Quiescent control and MYC-RALT–expressing NR6-EGFR Dc214 cells were either left untreated or stimulated with 20 ng/ml EGF for 10 min at 37°C. Cells were fixed and stained with anti-EGFR mAb 108 (red) and Hoechst 33258 (blue). (B) MYC-RALT–expressing NR6-EGFR Dc214 cells were rendered quiescent and then incubated with 20 ng/ml EGF on ice for 30 min. After EGF wash-out, cells were chased at 37°C in EGF-free medium for 10 min, fixed, and stained for EGFR, EEA1, and MYC-RALT immunodetection. Nuclei were stained with Hoechst 33258 (blue). (C) NR6-EGFR Dc214 cells were transfected with either control or RALT-specific siRNAs. Cells were made quiescent by serum deprivation and then challenged with 10% newborn calf serum (NCS) for 3 h to induce RALT protein expression. After serum wash-out, cells were left untreated or stimulated with 20 ng/ml EGF for 10 min at 37°C before being processed for anti-EGFR staining (red). Nuclei were stained with Hoechst 33258 (blue). Sister cultures were lysed to monitor the efficiency of RALT KD by immunoblot (top). Nontransfected NR6-EGFR Dc214 cells (±NCS stimulation) were included as additional immunoblotting controls. β-Actin was used as loading control. (D) Control and RALT siRNA-transfected NR6 Dc214 cells were made quiescent and then stimulated with NCS as in C. After serum wash-out, cells were incubated with 1 ng/ml [^{125}I]-EGF for 8 min at 37°C. Nontransfected cells (±NCS stimulation) were included as additional control. Columns report the average of three independent experiments ± SD. Bars: (A and C) 20 µm; (B) 5 µm.

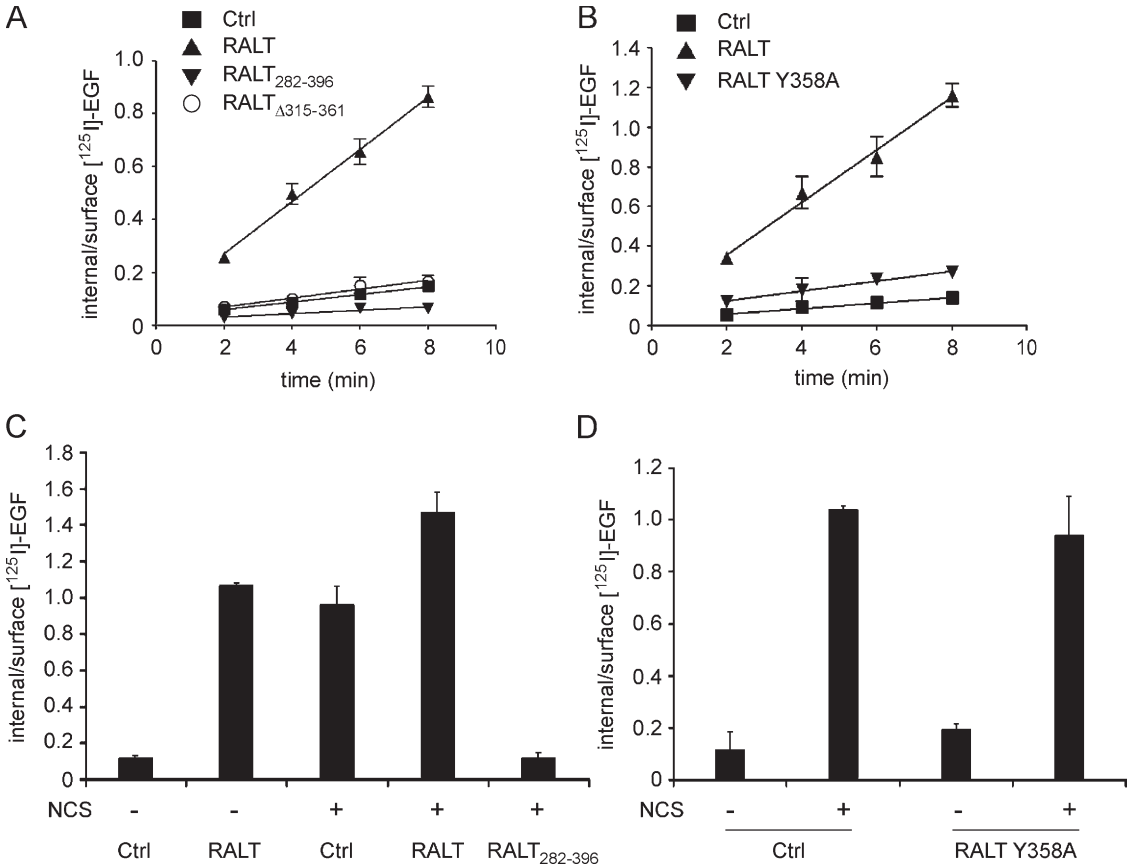

Figure 3. **Relocation onto EGFR is required for RALT-mediated endocytosis.** (A and B) Quiescent NR6-EGFR Dc214 cells expressing the indicated MYC-RALT alleles were assayed for [^{125}I]-EGF uptake (1 ng/ml at 37°C for the indicated time). The graphs report average results ± SD from four (A) and three (B) independent experiments. (C and D) NR6-EGFR Dc214 cells expressing the indicated MYC-RALT alleles were made quiescent and then assayed for [^{125}I]-EGF uptake (1 ng/ml for 8 min at 37°C) either before or after a 3-h stimulation with 10% NCS to induce RALT expression. Results were averaged ± SD from three independent experiments. Comparison between endogenous and ectopic RALT proteins indicates that the latter are largely overexpressed (see Fig. S2 A), thus allowing the assessment of their potential dominant-negative activity over endogenous RALT.

instead observed in cells exposed to the EGF pulse (Fig. 2 C). Crucially, endocytosis of EGFR Dc214 was abrogated by knock-down (KD) of RALT (Fig. 2 C). [^{125}I]-EGF uptake assayed in the same conditions confirmed that RALT-specific RNAi reduced EGFR Dc214 endocytosis to background levels (Fig. 2 D). Of note, RALT KD altered neither transferrin uptake in serum-stimulated NR6-EGFR Dc214 cells (Fig. S1 C) nor wtEGFR endocytosis in serum-stimulated NR6-EGFR cells (Fig. S1, D and E). We conclude that RALT KD does not cause a general disruption of endocytosis and that under physiological conditions RALT-bound and RALT-free EGFR molecules are internalized with comparable efficiency.

Identification of an endocytic domain in the RALT protein

To identify the structural determinants of RALT required for RALT-mediated endocytosis we focused initially on the region that contacts the EGFR kinase domain, namely the EBR module that spans positions 323–411 (X. Zhang et al., 2007). Because we could not express RALT$_{323–411}$ in NR6-Dc214 cells at suitable levels, we resorted to using RALT$_{282–396}$, which we showed was sufficient to suppress EGFR kinase activity (Anastasi et al., 2007). RALT$_{282–396}$, as well as two mutants unable to bind to EGFR, namely RALT Y358A (X. Zhang et al., 2007) and RALT Δ315-361 (Anastasi et al., 2007), did not support endocytosis of EGFR Dc214 (Fig. 3, A and B; expression levels of MYC-tagged RALT proteins are shown in Fig. S2 A). These results suggest that binding to EGFR is necessary but not sufficient for RALT-mediated endocytosis. Indeed, overexpressed RALT$_{282–396}$, but not RALT Y358A, displayed dominant-negative activity toward endogenous RALT in EGFR Dc214 internalization assays (Fig. 3, C and D), most likely because it prevented recruitment of endogenous RALT to EGFR Dc214.

Based on the above results, we hypothesized that relocation of RALT onto the EGFR via the EBR enables structural determinants of RALT distinct from the EBR itself to be connected to the endocytic machinery. This model predicts that RALT should mediate endocytosis independently of its EBR when placed in cis to EGFR$_{1–682}$, namely to an EGFR lacking both the kinase domain and C-terminal tail (Fig. 4 A). The 144–411 fragment of RALT spans the evolutionarily conserved region of the protein (Anastasi et al., 2007) and was capable of driving efficient down-regulation of EGFR Dc214 (Fig. S2 B). Strikingly, a chimera spanning the RALT 144–411 fragment fused to the C-terminal end of EGFR$_{1–682}$ (ER$_{144–411}$) underwent rapid endocytosis when expressed in NR6 cells (Fig. 4 B).

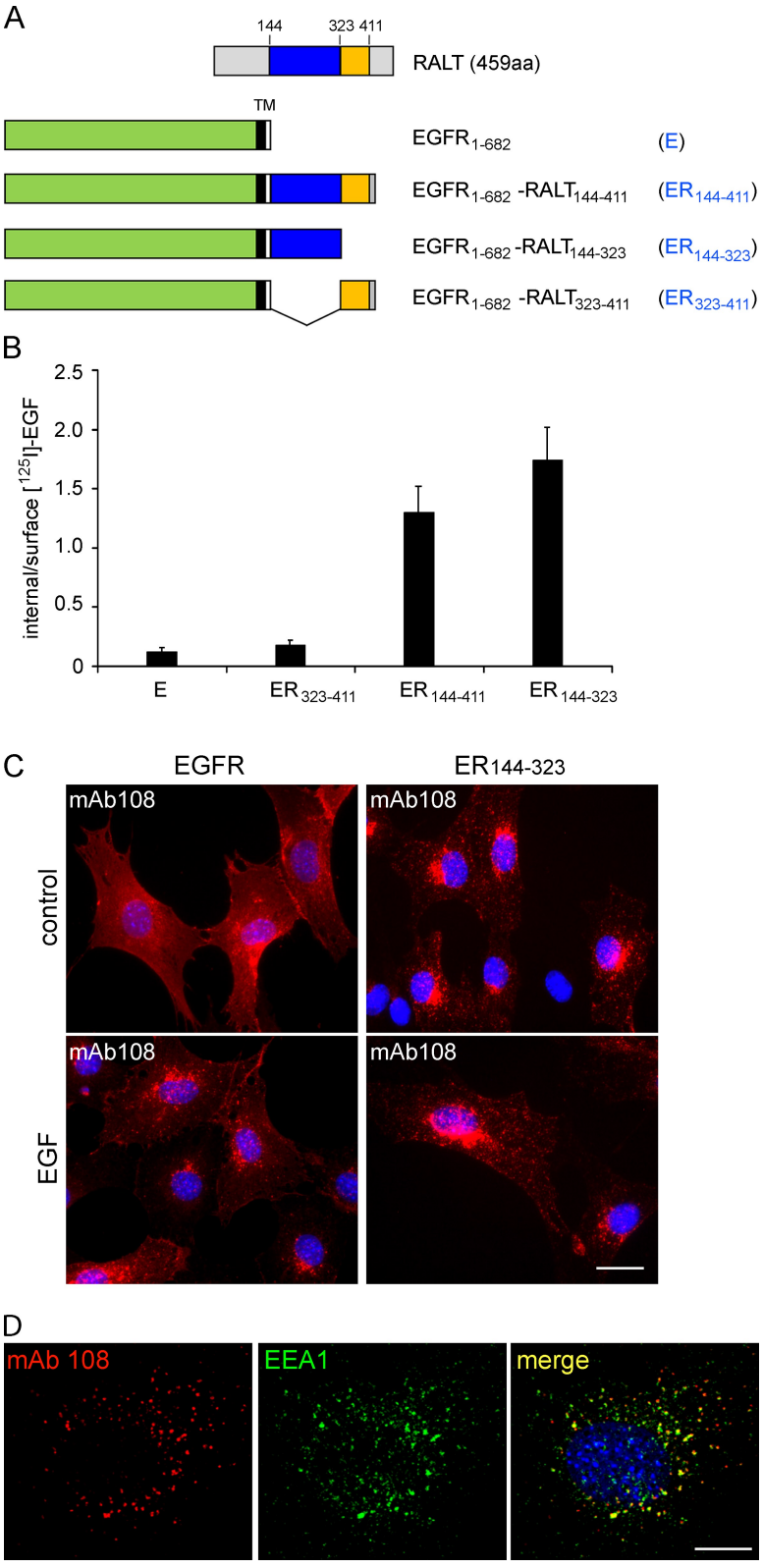

Figure 4. **Identification of the RALT endocytic domain.** (A) Schematic representation of chimeras generated by fusing the indicated fragments of RALT to the C-terminal end of $EGFR_{1–682}$. (B) The indicated $EGFR_{1–682}$-RALT chimeras (referred to as ER, see panel A) were expressed in NR6 cells. Quiescent cells were assayed for [^{125}I]-EGF uptake (3 ng/ml for 5 min at 37°C). Columns report average results ± SD from four independent experiments. (C) Quiescent NR6 cells expressing either wt EGFR or $ER_{144–323}$ were allowed to bind mAb 108 (3 µg/ml) for 30 min on ice either in the absence or presence of EGF (20 ng/ml). After mAb wash-out, cells were shifted to 37°C in mAb/EGF-free medium for 10 min. After fixation, cells were stained with anti–mouse IgG to visualize mAb 108 (red) and Hoechst 33258 (blue). (D) Quiescent NR6-$ER_{144–323}$ cells were incubated for 30 min on ice with 3 µg/ml mAb 108. After mAb wash out, cells were chased for 10 min at 37°C in serum-free medium before being processed for mAb 108 and EEA1 immuno-imaging. Nuclei were stained with Hoechst 33258 (blue). Bars: (C) 20 µm; (D) 5 µm.

The EBR-containing chimera ($ER_{323–411}$) behaved similarly to $EGFR_{1–682}$ and was not internalized. The endocytic determinants of RALT were mapped to the $RALT_{144–323}$ fragment because the $ER_{144–323}$ chimera was internalized as efficiently as $ER_{144–411}$ (Fig. 4 B). Thus, the RALT 144–323 fragment was named RED (RALT endocytic domain).

To assess whether the endocytosis of the RED-containing chimera was still EGF inducible, we used as endocytic tracer the mAb 108, which recognizes the EGFR extracellular domain independently of EGF binding (see Materials and methods). Results presented in Fig. 4 C show that mAb 108 was internalized in NR6 cells expressing the $ER_{144–323}$ chimera irrespective

of EGF stimulation and was routed to the endosomal compartment (Fig. 4 D). This constitutive internalization is specific because the intracellular accumulation of mAb 108 in NR6-EGFR cells was strictly dependent on EGF stimulation.

The experiments presented in Figs. 3 and 4 indicate that kinase suppression and endocytic activity are genetically separable functions of RALT that map to two distinct modules, i.e., the EBR and RED, respectively.

RALT signals degradation of EGFR

Internalized EGFR can either be recycled to the cell surface or further trafficked to lysosomes for degradation. While recycling favors reiteration of EGFR signaling (Lenferink et al., 1998; Sigismund et al., 2008), sorting into MVBs terminates it and, by causing receptor degradation, also attenuates the cell's responsiveness to further stimulation by EGFR ligands (Marmor and Yarden, 2004).

As shown before, RALT-bound EGFR molecules undergo down-regulation and degradation (Fig. 1, C and D). RALT also promoted down-regulation (Fig. 5 A and Fig. S2 C) and degradation of EGFR Dc214, as extrapolated by the observation that a sizeable amount of input [^{125}I]-EGF underwent degradation in NR6-EGFR Dc214/RALT cells (Fig. 5 B and Fig. S2 D). Consistently, EGFR Dc214–RALT complexes trafficked to anti-LAMP1–labeled endosomes (Fig. 5 C). Thus, besides rescuing the internalization deficit of EGFR Dc214, RALT was also capable of routing internalized EGFR Dc214 to late endosomes.

Trafficking toward the MVBs and consequent lysosomal degradation depend on CBL-driven EGFR ubiquitylation. The EGFR Y1045F mutant lacks the phosphotyrosine binding site for CBL. As a consequence, EGFR Y1045F is ubiquitylated poorly and is recycled to the cell surface rather than being sorted into MVBs/late endosomes (Levkowitz et al., 1999). Strikingly, RALT overexpression rescued the degradation deficit of EGFR Y1045F. Comparable results were obtained when the expression of EGFR Y1045F and RALT was reconstituted either stably in NR6 fibroblasts (Fig. 5 D) or transiently in CHO epithelial cells (Fig. S3 A). Notably, RALT-driven degradation of EGFR Y1045F was inhibited in cells treated with chloroquine (Fig. 5 D), pointing to lysosomes as the site of RALT-dependent degradation of EGFR. Neither RALT$_{282–396}$ (Fig. S3 A) nor RALT$_{323–411}$ (Fig. S3 B) was capable of rescuing the degradation deficit of EGFR Y1045F. In contrast, RALT$_{144–411}$ induced degradation of both wtEGFR (Fig. S2 E) and EGFR Y1045F (Fig. S3 B). Thus, the RED mediates internalization as well as degradation of EGFR.

The ubiquitylation deficit imposed on EGFR by the Y1045F mutation was not rescued by the ectopic expression of RALT (Fig. 5 E). This is consistent with the notion that binding of CBL to the EGFR requires receptor autophosphorylation (Levkowitz et al., 1998, 1999), which is abolished by RALT-mediated kinase inhibition. Indeed, also in the case of wtEGFR, RALT inhibited recruitment of CBL to the receptor as well as EGFR ubiquitylation (Fig. S3 C). The above data indicate that RALT-bound EGFR molecules undergo degradation into lysosomes in the absence of receptor ubiquitylation.

RALT couples the EGFR to clathrin-dependent endocytosis via AP-2

Several mechanisms of internalization were discovered for EGFR (Orth and McNiven, 2006; Acconcia et al., 2009; Sorkin and Goh, 2009). RALT colocalized with clathrin heavy chain (CHC) upon EGF stimulation (Fig. 6 A). CHC KD in NR6-EGFR Dc214 cells abolished [^{125}I]-transferrin uptake as well as RALT-mediated uptake of [^{125}I]-EGF (Fig. 6 B). In keeping with these results, RALT-dependent endocytosis of EGFR Dc214 required dynamin2, a GTPase implicated in the formation and fission of clathrin-coated structures at the plasma membrane (Macia et al., 2006; Loerke et al., 2009), as shown by the inhibitory activity exerted by both K44A DYN2, a dominant-negative dynamin2 mutant, and dynasore, a reversible inhibitor of dynamin GTPase activity (Macia et al., 2006; Fig. 6, C and D).

AP-2 is the major adaptor complex involved in CME and binding to AP-2 allows cargos to be sorted into CCPs (Traub, 2009). Depletion of the μ2 chain of the AP-2 complex resulted in marked inhibition of RALT-dependent endocytosis of EGFR Dc214. This effect was proportional to the extent of μ2 depletion as determined by two different siRNAs (Fig. 6 E). Purified recombinant GST-RALT$_{145–414}$ immobilized onto agarose beads was able to bind to AP-2 present in cell lysates, as assessed by immunoblotting with antibodies to β2 and μ2 chains of AP-2, whereas RALT$_{325–414}$ did not (Fig. S4 A). Hence, binding of RED to AP-2 may sort EGFR–RALT complexes into CCPs.

Role of Intersectin in RALT-dependent endocytosis

A number of endocytic proteins, including several accessory proteins, contain one or more Src homology 3 (SH3) domains (Simpson et al., 1999; Praefcke et al., 2004). We have previously shown that RALT binds to SH3 domains, with most of the SH3-binding motifs being located in the 144–323 sequence (Fiorentino et al., 2000). We therefore sought to determine whether RALT couples to SH3-containing proteins implicated in endocytic traffic. By combining computational predictions and literature-generated hypotheses we restricted our attention to SH3 domains present in ∼20 mammalian proteins. GST pull-down assays indicated that recombinant SH3 domains from GRB2, βPIX/Cool1, Intersectin1, and Intersectin2 (mammals express two ITSN isoforms encoded by distinct loci; see Pucharcos et al., 2001) bound RALT with the highest affinity (Fig. S4 B). We used RNAi to test whether the loss of GRB2, βPIX, or ITSNs impacts RALT-mediated endocytosis. Although GRB2 and βPIX are dispensable for RALT-driven endocytosis of EGFR Dc214 (Fig. S4, C and D), ITSN function appears to be necessary. In particular, the KD of ITSN2 reduced EGFR Dc214 endocytosis by ∼40% (Fig. 7 A). RNAi to *ITSN1* produced a minor, albeit reproducible, reduction of EGFR Dc214 internalization, which was additive to the effect of RNAi to *ITSN2* in combined ITSN1 + ITSN2 KD experiments (Fig. 7 A). ITSN2 KD had no consequence on the endocytosis of wtEGFR (Fig. S4 E), which was instead compromised by GRB2 KD, as reported previously (Jiang et al., 2003; Fig. S4 C). Thus, RALT-dependent and RALT-independent endocytosis of EGFR have

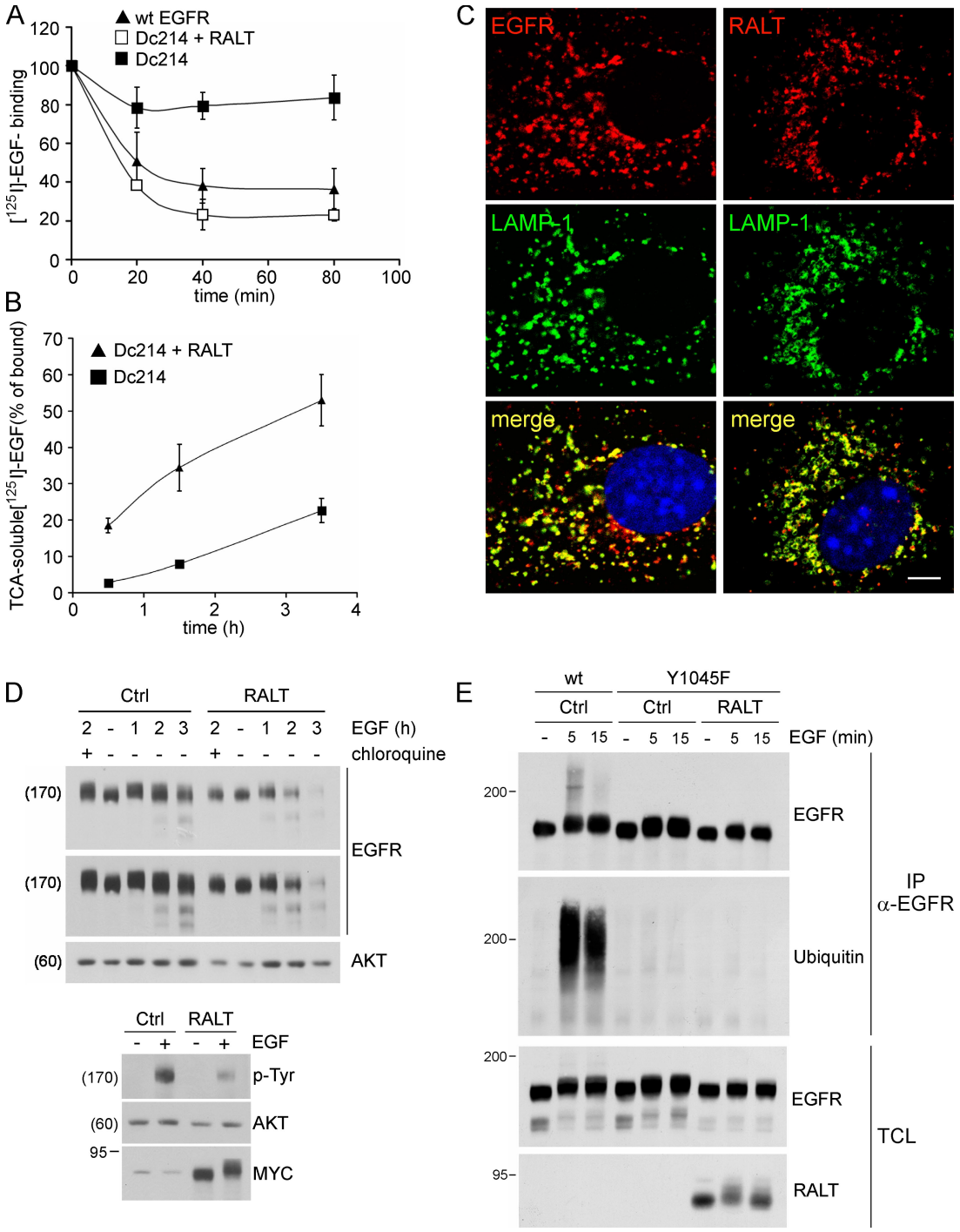

Figure 5. **RALT drives degradation of EGFR Dc214 and EGFR Y1045F.** (A) EGFR Dc214 down-regulation. Control and MYC-RALT–expressing NR6-EGFR Dc214 cells were made quiescent and assayed for receptor down-regulation as in Fig. 1 C. Graphs indicate the average results ± SD from three independent experiments. (B) [^{125}I]-EGF degradation. Quiescent control and MYC-RALT–expressing NR6-EGFR Dc214 cells were allowed to bind [^{125}I]-EGF on ice (15 ng/ml for 45 min). After washing, cells were shifted to 37°C in EGF-free medium for the indicated time. Degraded [^{125}I]-EGF was measured as the fraction of TCA-soluble radioactivity (i.e., the sum of TCA-soluble cpm measured in cell lysates and extracellular medium) over bound [^{125}I]-EGF. Results were averaged (±SD) from three independent experiments. Note that under these conditions EGF stimulation induces significant RALT expression in control NR6-EGFR Dc214 cells by 90 min (not depicted), which likely explains why in control cells [^{125}I]-EGF degradation increases above background past the 1.5-h time point. (C) Quiescent MYC-RALT–expressing NR6-EGFR Dc214 cells were incubated with EGF on ice as in Fig. 2 B, washed, chased in EGF-free medium for 30 min at 37°C, and processed for EGFR, LAMP-1, and MYC-RALT immuno-imaging. Nuclei were stained by Hoechst 33258. (D) Top: control and MYC-RALT–expressing NR6-EGFR Y1045F cells were made quiescent and then stimulated with 100 ng/ml EGF for the indicated time. Where indicated, chloroquine was added to the culture medium throughout the EGF incubation time. Lysates were immunoblotted with the indicated antibodies. Two different exposures of the same anti-EGFR autoradiograph are shown. Bottom: sister plates were stimulated with 100 ng/ml EGF for 5 min at 37°C to document the extent of catalytic suppression of EGFR Y1045F by MYC-RALT. Blots were probed as indicated; AKT was used as loading control. (E) NR6 fibroblasts expressing either wtEGFR or EGFR Y1045F in the absence (Ctrl) or presence of ectopic MYC-RALT (RALT) were made quiescent and either left untreated or incubated with 20 ng/ml EGF for the indicated time (min). Anti-EGFR immunoprecipitates and total cell lysates were immunoblotted as indicated. Bar, 5 µm.

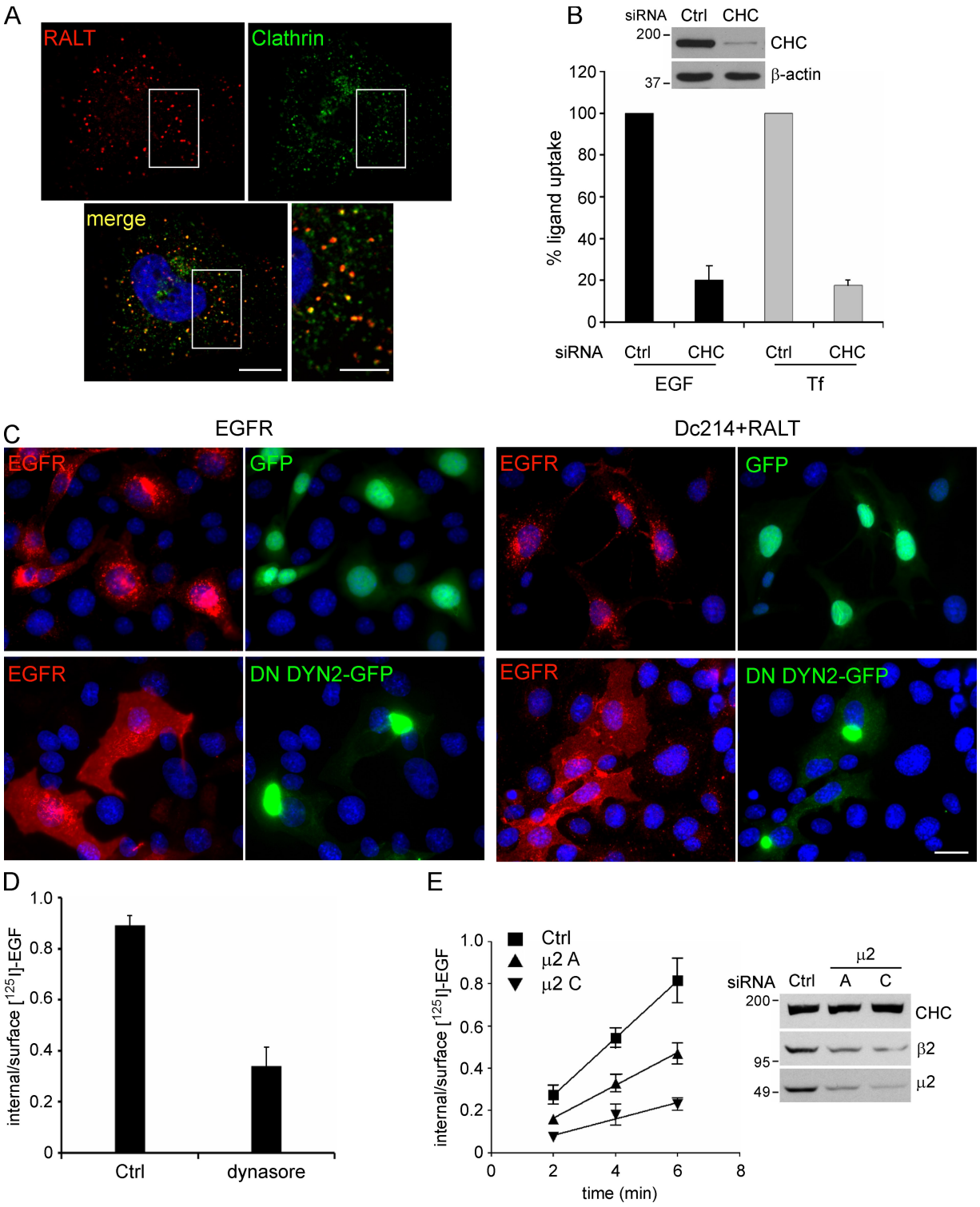

Figure 6. **RALT-mediated endocytosis is clathrin- and AP-2–dependent.** (A) MYC-RALT–expressing HeLa cells were made quiescent and then incubated with 20 ng/ml EGF for 5 min at 37°C before MYC-RALT and CHC immunostaining. (B) NR6-EGFR Dc214 RALT cells were transfected with control and CHC-specific siRNAs. Cells were rendered quiescent and assayed for [^{125}I]-EGF (1 ng/ml for 6 min at 37°C) and [^{125}I]-Tf (0.5 μg/ml for 4 min at 37°C) uptake. Results were averaged ± SD from four independent experiments. The immunoblot documents the typical efficiency of CHC KD; β-actin was used as loading control. (C) CHO cells were transfected with either GFP or dominant-negative (DN) DYN2 K44A-GFP vectors along with either pcDNA3-EGFR + pCS2MT (left) or pcDNA3-EGFR Dc214 + pCS2MT-RALT (right). 2 d after transfection, cells were made quiescent and stimulated with 20 ng/ml EGF for 10 min at 37°C before being processed for anti-EGFR staining. Nuclei were stained with Hoechst 33258 (blue). (D) Quiescent NR6-EGFR Dc214 cells were incubated for 30 min at 37°C with either vehicle or 80 μM dynasore before being assayed for [^{125}I]-EGF uptake (± dynasore) for 6 min at 37°C. Results were averaged ± SD from three independent experiments. (E) NR6-EGFR Dc214 cells were transfected with control and two different μ2-specific siRNAs. Cells were made quiescent and assayed for [^{125}I]-EGF uptake (1 ng/ml for the indicated time at 37°C). Results were averaged ± SD from three independent experiments. The immunoblot documents μ2 KD, which causes also concomitant reduction of the β2 subunit, as reported previously (Johannessen et al., 2006); CHC was used as loading control. Bars, (A) 10 μm; (inset) 5 μm; (C) 20 μm.

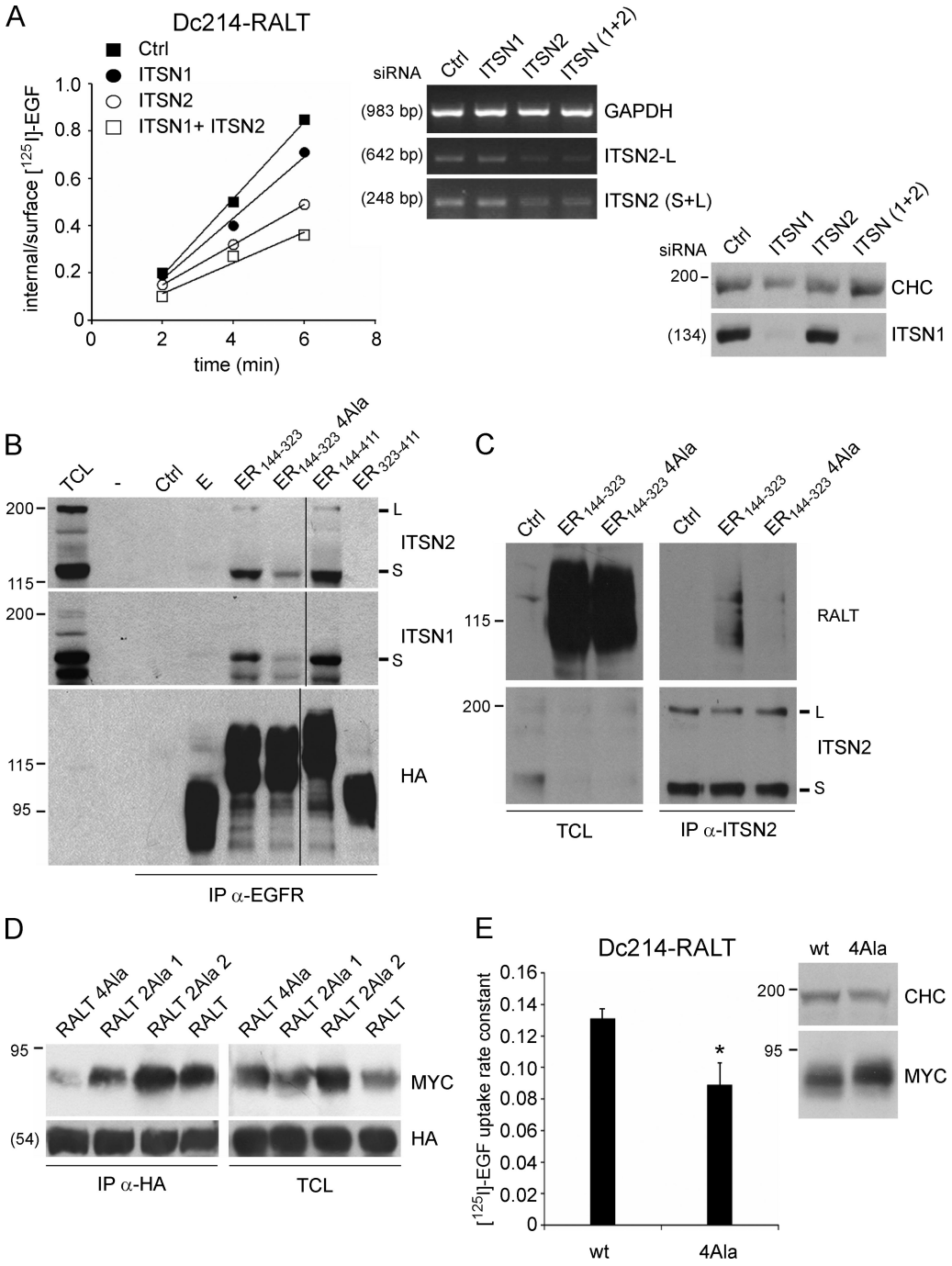

Figure 7. **ITSN recruitment by RALT is necessary for RALT-mediated endocytosis.** (A) NR6-EGFR Dc214 cells were transfected with either control or ITSN-specific siRNAs. Cells were made quiescent before being tested for [^{125}I]-EGF uptake (1 ng/ml for the indicated time at 37°C). An experiment representative of three independent experiments is shown. ITSN KD efficiency was documented by immunoblot (ITSN1, bottom) and RT-PCR (ITSN2, top; note that our anti-ITSN2 antibody does not react against the mouse protein). GAPDH was used as RT-PCR reaction control. (B and C) HEK 293 cells were transfected with either empty vector (Ctrl) or vectors directing the expression of the indicated EGFR$_{1–682}$-RALT chimeras. Lysates were subjected to immunoprecipitation with anti-EGFR mAb 108 (B) and anti-ITSN2 antiserum (C). Total cell lysates (TCL, 5% of input lysate in IPs) and IPs were immunoblotted as indicated. (D) HEK 293 cells were cotransfected with vectors encoding HA-tagged 5SH3 *X. laevis* ITSN and the indicated MYC-RALT alleles. Cell lysates were immunoprecipitated with anti-HA antibodies and immunoblotted with anti-MYC 9E10 mAb. (E) EGFR Dc214 cells expressing comparable amounts of either wt or MYC-RALT 4Ala (see immunoblot) were made quiescent and assayed for [^{125}I]-EGF uptake (1 ng/ml at 37°C). Columns report the endocytic rate constants K_e averaged from three independent experiments (0.131 ± 0.006 for wtRALT and 0.099 ± 0.013 for RALT 4Ala, P = 0.039).

differential requirements for GRB2 and ITSN2 function, at least in NR6 fibroblasts.

The prevalent isoforms of ITSN1 and ITSN2 have a modular architecture consisting of two EH domains, a centrally located coiled-coil region, and five SH3 domains (denominated A through E; O'Bryan et al., 2001). RALT bound in vitro to SH3 A, C, and E of ITSN (Fig. S5 A) and coimmunoprecipitated specifically with a fragment of ITSN spanning the five

SH3 domains (Fig. S5 B). Binding of RALT to ITSN required the RED: GST-RALT$_{145–414}$, but not GST-RALT$_{325–414}$, precipitated endogenous ITSN1 and ITSN2 from cell lysates (Fig. S5 C). Moreover, endogenous ITSN1 and ITSN2 coimmunoprecipitated only with the ER$_{144–323}$ chimera in mAb 108 immunoprecipitations (Fig. 7 B); reciprocally, anti-ITSN2 antibodies brought down ER$_{144–323}$ (Fig. 7 C).

SH3 domains recognize a PXXP core sequence flanked by a positively charged amino acid (+) in either class I (+XXPXXP) or class II (PXXPX+) orientation (Mayer, 2001). Several PXXP sequences are clustered within the RED between positions 278 and 322. Based on the probability score assigned by the Scansite program (http://scansite.mit.edu) to candidate ITSN binding motifs in RALT, we introduced Ala substitutions in the $_{279}$PEIPPR$_{284}$ and $_{315}$PKVPPR$_{320}$ RALT sequences (underlined residues were changed to A). As shown in Fig. 7 D, RALT lost the ability to coimmunoprecipitate with a recombinant protein spanning the five SH3 domains of *Xl*ITSN when both of the above PXXPXR sequences were mutated (RALT 4Ala). GST-5SH3 recombinant proteins from either ITSN1 or ITSN2 lost the ability to interact with RALT 4Ala (Fig. S5 D). Finally, the 4Ala mutation strongly reduced the interaction between the ER$_{144–323}$ chimera and ITSNs (Fig. 7, B and C). Strikingly, RALT 4Ala showed a significant reduction in the ability of driving EGFR endocytosis as measured by [^{125}I]-EGF uptake (Fig. 7 E; Fig. S5 E). We note that combined RNAi to *ITSN1* and *ITSN2* had a stronger effect than the 4Ala mutation on EGFR Dc214 endocytosis, possibly because 4Ala mutants displayed some residual binding to ITSNs (Fig. 7, B–D).

The sum of the above results supports a model whereby the endocytic domain of RALT couples EGFR to CME via its interaction with AP-2 and Intersectins.

Discussion

Ligand-activated EGFR drives its own endocytic traffic by interacting with endocytic proteins. This network of protein–protein interactions is activated by post-translational modifications of the EGFR, i.e., tyrosine phosphorylation and ubiquitylation, which are induced and maintained by EGFR kinase activity. Hence, EGFR endocytic traffic is intimately connected to receptor activation (Sorkin and Goh, 2009). Deviating from this consolidated notion, we show here that RALT-bound EGFR molecules are internalized and eventually delivered to lysosomes for degradation in the absence of EGFR kinase activity.

RALT rescues the endocytic deficit of EGFR mutants unable to undergo either internalization (EGFR Dc214) or sorting from early endosomes into MVBs (EGFR Y1045F). The endocytic activities of RALT map to the 144–323 sequence, which we called RED. The isolated EBR domain phenocopies the inhibitory activity of AG1478, not supporting EGFR endocytosis. A functional EBR is nevertheless required for RALT-mediated endocytosis because it provides the docking function necessary to relocate cytosolic RALT in proximity of the endocytic machinery. We posit that RALT mediates EGFR endocytosis thanks to its ability of acting as a scaffold for components of the endocytic machinery.

Our results clearly show that RALT-dependent endocytosis of EGFR is clathrin- and AP-2–dependent. RALT binds to the AP-2 complex and we suggest that this interaction is key to sorting EGFR–RALT complexes into CCPs. Binding of RALT to AP-2 requires determinants located within the RED. Two evolutionarily conserved sequences are present in the RED, namely $_{178}$DTDFLL$_{183}$ (which fits well with the [DE]XXXL[LIM] consensus for binding to the α:σ2 hemi-complex of AP-2) and $_{209}$YAYF$_{212}$ (conforming to the YXXΦ consensus for binding to the μ2 chain of AP-2; Traub, 2009). Further experiments are needed to evaluate their possible involvement in the RALT–AP-2 interaction.

RALT interacts functionally and physically with the accessory proteins ITSN1 and ITSN2, which are thought to be important for promoting maturation of cargo-loaded CCPs (Mettlen et al., 2009). ITSNs scaffold several components of the endocytic machinery, including AP-2 (Praefcke et al., 2004; Schmid et al., 2006), Epsin, EPS15 (Sengar et al., 1999), dynamin (Yamabhai et al., 1998), CIN85 (Nikolaienko et al., 2009), and CBL (Martin et al., 2006). The ITSN–RALT interaction is mediated by the SH3 domains of ITSNs and Pro-rich sequences located in the RED. As proved by RNAi experiments, ITSN1 and ITSN2 serve nonredundant functions in RALT-dependent endocytosis, with ITSN2 playing a prevalent role. Inhibiting the RALT–ITSNs interaction by the 4Ala mutation was likewise effective in reducing the rate of EGFR Dc214 endocytosis, supporting the notion that the RALT–ITSNs physical interaction is required for RALT-dependent CME.

The remarkable requirement of RALT-driven endocytosis for ITSN2 highlights mechanistic differences between the CME of kinase-active EGFR, which was insensitive to ITSN2 KD, and that of EGFR–RALT complexes. RALT-bound EGFR molecules lack ubiquitylation and are therefore unable to recruit accessory proteins containing ubiquitin-interacting motifs, i.e., EPS15, Epsin, and EPS15R (Traub, 2009). RALT may alleviate this deficit by recruiting ITSNs via SH3-directed interactions and we propose that ITSNs, as accessory protein recruited directly by RALT, could play a major role in driving the maturation of CCPs loaded with EGFR–RALT complexes (Mettlen et al., 2009). Given their ability to engage in multivalent interaction with the α2 and β2 subunit of the AP-2 complex, ITSNs have been proposed to function also as accessory cargo adaptors (Schmid et al., 2006) and could therefore enhance AP-2–dependent sorting of EGFR–RALT complexes into nascent CCPs. Our results also raise the issue of why ITSN2 has a prevalent role over ITSN1 in RALT-mediated endocytosis. This may be explained by the higher affinity of ITSN2 SH3 domains for RALT (Fig. S5 D). The long isoforms (ITSN-L) of ITSNs also couple endocytosis to actin remodelling (Hussain et al., 2001; McGavin et al., 2001). Whereas ITSN1-L is restricted to neuronal cells, ITSN2-L is expressed ubiquitously (Pucharcos et al., 2001). Thus, in nonneuronal cells, ITSN2-L could contribute a signaling function crucial to RALT-dependent endocytosis.

The RED is also required for directing EGFR into late endosomes independently of EGFR ubiquitylation. Our results show that RALT rescues the degradation, but not the ubiquitylation, deficit of EGFR Y1045F. This finding underscores

another important mechanistic difference between the endocytic traffic of kinase-active EGFR and that of EGFR–RALT complexes. Cargo sorting into late endosomes in the absence of cargo ubiquitylation has been described and may be distinguished from ubiquitin-dependent sorting on the basis of differential requirements for components of the ESCRT machinery (Hislop et al., 2004). We observed that RALT-driven degradation of EGFR was consistently slower than that of kinase-active EGFR (Fig. 1 D), even though the rates of EGFR down-regulation were similar in control and RALT-expressing cells. We suppose that this may be due to delayed sorting of RALT-bound EGFR molecules into the degradative compartment (in the absence of significant recycling to the cell surface; see Fig. S2 C), which in turn could reflect mechanistic differences between Ub-dependent and Ub-independent sorting of EGFR into MVBs. It must be noted that such a delay is not detrimental to RALT-dependent suppression of EGFR signaling, given that intracellular retention of EGFR by RALT is associated to catalytic repression of the receptor. Further studies are required to unveil the mechanistic details of RALT-dependent trafficking of EGFR to late endosomes.

Concluding remarks

The two-tiered mechanism of EGFR suppression enforced by RALT has important implications to cell regulation and tumor suppression. RALT is expressed in mid to late G1, i.e., when sustained mitogenic signals are necessary to activate the cell cycle machinery and direct the abundant RNA and protein synthesis required for cell size increase. Within this timeframe RALT concurs in determining whether EGFR mitogenic signals reach the threshold sufficient for G1 completion (Anastasi et al., 2005; Reschke et al., 2009). The present study indicates that EGFR kinase inactivation by RALT is associated to RALT-mediated receptor down-modulation. The two inhibitory mechanisms act sequentially: kinase blockade is synchronous with ligand binding, whereas EGFR down-regulation reduces receptor expression and therefore attenuates responsiveness to subsequent EGF stimulation. We propose that this temporally dilated attenuation of EGFR activation is key to determining that only cells receiving a robust enough EGF signal are eventually licensed to enter S phase.

RALT endocytic activity is also predicted to protect cells from oncogenic EGFR signaling. Oncogenic activation of EGFR is associated to, and also dependent on, reduced rates of receptor down-regulation. This may be caused by a variety of mechanisms, all of which seem to converge on quelling CBL-dependent EGFR ubiquitylation (Mosesson et al., 2008). Our data suggest that RALT may exert a potent tumor suppressor function not only through EGFR kinase suppression, but also by restoring down-regulation of oncogenic EGFR molecules that escape ubiquitylation and thus phenocopy the Y1045F mutant.

Materials and methods

Media, chemicals, and antibodies

Tissue culture media and sera were from Invitrogen and BioWhittaker. All chemicals were obtained from Sigma-Aldrich, unless specified otherwise. ECL, sepharose-coupled protein A and protein G, and agarose-coupled glutathione were from GE Healthcare. Nitrocellulose and PVDF membranes were from Schleicher and Schuell. EGF was from Millipore, tetramethylrhodamine-EGF and tetramethylrhodamine-transferrin conjugates were from MDS Analytical Technologies. Rabbit polyclonal anti-EGFR and anti–c-Myc antibodies, goat polyclonal antibody to EEA1, and mAb P4D1 anti-Ub and anti-GRB2 were purchased from Santa Cruz Biotechnology, Inc. Anti-pEGFR antibodies, anti-pERK, anti-pAKT, anti-ERK, and anti-AKT were from Cell Signaling Technology. The anti-βPIX antibody was from Millipore. Anti-CHC (human) (X22) was from EMD, rat antibody to mouse LAMP-1 was from eBioscence, and mAbs to adaptin β2 and μ2 were from BD. FITC- and TRITC-conjugated goat anti–rabbit and anti–mouse antibodies, donkey anti–goat, anti–mouse, anti–rabbit, and anti–rat were from Jackson ImmunoResearch Laboratories, Inc. HRP-conjugated goat anti–mouse and anti–rabbit antibodies were from Bio-Rad Laboratories. mAb 108 (anti-EGFR), 12CA5 (anti HA), and 9E10 (anti-MYC) were purified in house from hybridoma supernatants. Antibodies to ITSN1 and ITSN2 were raised in rabbits against recombinant proteins spanning positions 583–888 of hITSN1 and 618–885 of hITSN2 and purified by affinity chromatography. Anti-RALT affinity-purified HOR3 antibody (rabbit) was described previously (Anastasi et al., 2007). The mAb 22D/8 was generated against human RALT and recognizes an epitope located in the 325–375 *Hs*RALT sequence.

Cell culture and transfection procedures

NR6 fibroblasts, which lack endogenous EGFR (Pruss et al., 1978), were obtained from American Type Culture Collection and grown in DME containing 10% (vol/vol) newborn calf serum. For serum starvation, cells were incubated in DME/Ham's F12 (1:1 mixture) containing 0.2% serum. HEK 293 cells and the Phoenix ecotropic packaging cell line cells were grown in DME containing 10% fetal calf serum. Plasmid DNAs and siRNAs were transfected with Lipofectamine 2000 (Invitrogen) according to the manufacturer's protocols. For biochemical studies, transfected HEK 293 cells were harvested 48–72 h after transfection. Phoenix cell culture supernatants containing recombinant retrovirus were harvested 48–72 h after transfection, filtered through a 45-μm disposable filter, added to 8 μg/ml polybrene, and incubated with target cells for 3–6 h.

Immunochemical procedures

For most of the experiments reported here, cells were lysed on ice in HNTG (50 mM Hepes, pH 7.5, 150 mM NaCl, 10% glycerol, 5 mM EGTA, and 1% Triton X-100) containing 0.1 mM sodium orthovanadate and protease inhibitors. Lysates were cleared of nuclei and debris by centrifugation. Protein concentration was measured with the BCA kit (Thermo Fisher Scientific). For IP/WB experiments aimed at detecting ubiquitin-conjugated proteins, cells were lysed either in RIPA buffer (50 mM Tris-HCl, pH 7.5, 150 mM NaCl, 1% Triton X-100, 0.1% SDS, and 0.5% sodium deoxycholate) or in boiling 1% SDS. In the latter case, chromosomal DNA was sheared by sonication and cleared lysates were diluted with nine volumes of HNTG before being subjected to immunoprecipitation.

For immunoprecipitation experiments, antibodies were coupled to either protein A or protein G (2–10 μg Ab/IP) and incubated with lysates at 4°C on a rocker. Immune complexes were washed with lysis buffer and eluted with boiling Laemmli buffer. GST pull-down assays were performed as described previously (Anastasi et al., 2007). In brief, recombinant proteins were solubilized by sonication of bacteria, resuspended in NETN buffer (20 mM Tris-HCl, pH 8.0, 100 mM NaCl, 1 mM EDTA, and 0.5% NP-40). Lysates were cleared by centrifugation and GST fusion proteins purified onto agarose-glutathione sepharose 4B beads. Cell lysates were added to beads and binding reactions were allowed to proceed at 4°C under continuous rotation. Beads were washed with HNTG, bound proteins were eluted by boiling in Laemmli buffer and processed for immunoblot analysis.

[^{125}I]-EGF binding studies

[^{125}I]-EGF and [^{125}I]-Tf were either purchased from PerkinElmer or generated using the IODO-GEN kit according to the supplier's protocols (Thermo Fisher Scientific). Specific activity of EGF was at least 1.5×10^5 cpm/ng. For binding studies, NR6 derivatives were plated at 4×10^4 cells/well in 24-well gelatin-coated plates. For each time point we used triplicate wells, with a fourth well being used to determine background binding in the presence of a molar excess of unlabeled EGF.

For measuring initial rates of [^{125}I]-EGF uptake cells, we used the protocol described by Sorkin et al. (1992). Cells were incubated with binding medium (BM; i.e., DME containing 0.2% BSA and 20 mM Hepes, pH 7.5) for 10 min in a water bath at 37°C. Binding was initiated by adding 0.3 ml/well of 1 ng/ml [^{125}I]-EGF in BM. At the end of binding time, plates were put on ice, washed three times with ice-cold PBS, and incubated for 5 min with 0.5 ml/well ice-cold elution buffer (0.5 M NaCl/0.2 M

CH_3COOH, pH 2.8). After an additional 1-min wash with elution buffer, cell monolayers were dried and lysed with 1N NaOH. Cell surface–associated cpm (eluted with elution buffer) and internal cpm (solubilized in NaOH) were determined separately from triplicate wells for each time point. Background binding was determined in parallel in a fourth well containing a 300-fold molar excess of unlabeled EGF. The internalization rate constant (K_e) corresponds to the linear regression coefficient of the internal/surface ratio of [^{125}I]-EGF binding plotted as a function of time (Sorkin et al., 1992), and was calculated using Prism4 software (GraphPad Software, Inc.).

Ligand uptake assays at single time points were performed as above, except that 3 ng/ml [^{125}I]-EGF was used when assaying ER chimeras. Variables were analyzed by Student's *t* test and a probability value of $P \leq 0.05$ was deemed statistically significant.

For EGFR down-regulation assays (Sigismund et al., 2008), cells were plated as above, serum-starved for 16 h, and then incubated with 100 ng/ml EGF at 37°C. Plates were then put on ice and rinsed with ice-cold PBS. After eluting cell surface–bound EGF with 0.5 M NaCl/0.2 M CH_3COONa, cells were rinsed twice with ice cold BM and incubated for 2 h on ice with BM containing a mixture of 30 ng/ml [^{125}I]-EGF + 70 ng/ml unlabeled EGF. Cells were washed three times with ice-cold PBS and lysed with 10 mM NaOH/1% SDS. Specific radioactivity was measured in triplicate wells for each time point after subtraction of background binding (determined in parallel in a fourth well incubated with a 500-fold molar excess of unlabeled EGF). Data obtained from EGF-stimulated were expressed as percentage of [^{125}I]-EGF binding, considering 100% the value measured in unstimulated cells (i.e., time 0). As an alternative, EGFR down-regulation was assessed after allowing binding of EGF to cells on ice. Cells were then washed with ice-cold DME and shifted at 37°C in EGF-free DME for various lengths of time. Residual [^{125}I]-EGF binding was assessed as described above.

For [^{125}I]-EGF degradation assays (Sigismund et al., 2008), cells were plated as above, serum starved for 16 h, and incubated for 45 min on ice with BM containing 15 ng/ml [^{125}I]-EGF. Cells were washed three times with ice-cold BM and then incubated at 37°C with 0.5 ml/well BM. At the end of the incubation time, plates were put on ice, the medium was harvested, and cells washed twice with ice-cold PBS. After eluting cell surface–associated [^{125}I]-EGF with a pH 2.8 wash (see above), cells were rinsed with PBS and lysed with 1 mM NaOH. TCA-soluble and TCA-insoluble radioactivity was determined in medium and cell lysates. The TCA-soluble radioactivity recovered at each time point in medium and cell lysates measured the fraction of degraded [^{125}I]-EGF and was expressed as percentage of total radioactivity bound to cells (medium + cell surface + internal).

RNA interference

NR6 derivatives were plated at 10^5 cells/35-mm dish and grown for 24 h. siRNAs were transfected for 6 h at a concentration of 50 nM using Lipofectamine. For CHC, ITSN1 and ITSN2 knock-down cells were transfected twice and analyzed 96 h after the first transfection cycle. Cells were transferred into 24 well plates for [^{125}I]-EGF binding studies 24 h after completing transfection procedures. A fraction of transfected cells was plated onto 35-mm dishes to monitor RNAi efficiency by WB or RT-PCR. Smart pool siRNAs directed against mouse GRB2, βPIX, and RALT were obtained from Thermo Fisher Scientific. Stealth siRNA directed against ITSN1 (5′-CAGCUGGCUUCAAUAUGGAAUCUUU-3′), ITSN2 (5′-GCAUGUCAUUGAAGCUACAGAAUUA-3′), μ2 chain of AP-2 (5′-CAAGCAAGAAGUGGUAAGCAGUCGAU-3′ and 5′-GCGACUCAGCAAGUUUGACUCUGAG-3′, denoted as A and C in the text, respectively) and CHC (5′-GAAGAACUCUUUGCCCGGAAAUUUA-3′) were obtained from Invitrogen.

Recombinant DNA

pcDNA3-EGFR, pcDNA3-EGFR$_{1–682}$, pcDNA3-EGFR Y1045F (Haglund et al., 2003; Sigismund et al., 2008), and pcDNA3-EGFR Dc214 (Levkowitz et al., 1998) have been described previously. pCS2-MT and pBabe-puro mammalian expression vectors for MYC-tagged rat RALT have been described previously (Anastasi et al., 2007). The Y358A mutation was generated in the human RALT cDNA. Human RALT cDNAs in wt and Y358 configuration were subcloned in pBabe puro vector to express MYC-tagged proteins. GST fusions spanning human RALT 145–414 and 325–414 were generated by PCR amplification of human RALT cDNA fragments followed by subcloning in the pGEX-6P vector. *Xenopus laevis* ITSN vectors were obtained from B. Kay (University of Illinois at Chicago, Chicago, IL) and have been described previously (Yamabhai et al., 1998). EGFR$_{1–682}$-RALT chimeras were generated by subcloning PCR-amplified fragments of RALT into pcDNA3-EGFR$_{1–682}$. EGFR$_{1–682}$/RALT chimeras were also subcloned in the pBabe-puro retroviral vector for stable expression in NR6 cells. Mutant (Dc214 and Y1045F) and wtEGFR cDNA clones were subcloned in pBabe-puro to obtain vectors suitable for the generation of recombinant retrovirus stocks. Fragments encoding the 5SH3 region of human ITSN1 and ITSN2 (Pucharcos et al., 2001) were amplified by PCR and subcloned into pGEX-6P. Site-directed mutagenesis was performed using the QuikChange kit (Agilent Technologies). RNA was extracted from cultured cells using Trizol (Invitrogen). Quantitative RT-PCR was performed with the Advantage kit (Takara Bio Inc.). Primers for mouse *ITSN2* were designed to amplify both short and long isoforms (primer sequences are available upon request).

Immunofluorescence analysis

For endocytosis studies, quiescent cells were incubated for 30 min at 4°C with EGF (20 ng/ml), washed with cold DME, and then shifted to 37°C for the indicated lengths of time in EGF-free DME. Cultures were routinely rinsed with PBS (+ Ca^{2+}/Mg^{2+}), fixed with 4% paraformaldehyde in PBS for 10 min, permeabilized with 0.25% Triton X-100 in PBS at 20°C, and processed with antibodies as described previously (Fiorentino et al., 2000; Ballarò et al., 2005). For LAMP1 labeling, cells were fixed with methanol at −20°C for 5 min. Cells were incubated with primary antibodies and subsequently with conjugated secondary antibodies in 1% RIA-grade BSA; finally, coverslips were mounted with Gelvatol. A similar protocol was adopted for endocytosis of TRITC-conjugated EGF (0.5 μg/ml EGF-TRITC) and transferrin (25 μg/ml transferrin-TRITC); cultures were then fixed with 4% paraformaldehyde and mounted for visualization. For CHC detection, cells were rinsed with ice-cold PBS (+ Ca^{2+}/Mg^{2+}) and fixed with ice-cold 4% paraformaldehyde. The samples were routinely examined with a microscope (model AX70; Olympus) equipped with a 40x/0.75 PH2 and 60x/1.40 oil objective lenses. Images were recorded on a CCD camera (SPOT; Diagnostic Instruments, Inc.) run by DeltaSystem software. Confocal microscopy was performed with a confocal microscope (TCS-SP; Leica) equipped with PLA 40x/1.25 and 60x/1.40 oil objectives. Colocalizations were recorded using sequential recording with line average. Recorded images were processed using Adobe Photoshop software (using linear curve correction for adjusting brightness and contrast to whole images; levels were adjusted equally for all images in a set) and ImageJ software.

Online supplemental material

Fig. S1 shows that RALT drives endocytosis and degradation of kinase-suppressed EGFR. Fig. S2 shows down-regulation/degradation of EGFR Dc214 by RALT as well as the endocytosis-inducing activity of the evolutionarily conserved 144–411 fragment of RALT. Fig. S3 shows that RALT rescues the degradation deficit of EGFR Y1045F independently of receptor ubiquitylation. Fig. S4 shows the analysis of SH3-containing proteins in RALT-mediated endocytosis. Fig. S5 analyzes the molecular bases of the RALT–ITSN physical interaction. Online supplemental material is available at http://www.jcb.org/cgi/content/full/jcb.201002032/DC1.

We are indebted to Y. Yarden, B. Kay, P.P. Di Fiore, S. Sigismund, S. Giordano, N. Vitale, S. de la Luna, G. Cesareni, and A. Sorkin for reagents and advice. We thank R. Fraioli for expert technical assistance and M.V. Sarcone for secretarial assistance. O. Segatto gratefully acknowledges the support of his colleagues at CRS.

O. Segatto is funded by grants from Fondo Italiano per la Ricerca di Base, Associazione Italiana per la Ricerca sul Cancro, and Progetto Integrato Oncologia. S. Alemà is supported by Progetto di Rilevante Interesse Nazionale/Ministero Italiano Università Ricerca.

We dedicate our work to the cherished memory of Eliana.

Submitted: 5 February 2010
Accepted: 2 April 2010

References

Acconcia, F., S. Sigismund, and S. Polo. 2009. Ubiquitin in trafficking: the network at work. *Exp. Cell Res.* 315:1610–1618. doi:10.1016/j.yexcr.2008.10.014

Amit, I., A. Citri, T. Shay, Y. Lu, M. Katz, F. Zhang, G. Tarcic, D. Siwak, J. Lahad, J. Jacob-Hirsch, et al. 2007. A module of negative feedback regulators defines growth factor signaling. *Nat. Genet.* 39:503–512. doi:10.1038/ng1987

Anastasi, S., L. Fiorentino, M. Fiorini, R. Fraioli, G. Sala, L. Castellani, S. Alemà, M. Alimandi, and O. Segatto. 2003. Feedback inhibition by RALT controls signal output by the ErbB network. *Oncogene.* 22:4221–4234. doi:10.1038/sj.onc.1206516

Anastasi, S., G. Sala, C. Huiping, E. Caprini, G. Russo, S. Iacovelli, F. Lucini, S. Ingvarsson, and O. Segatto. 2005. Loss of RALT/MIG-6 expression in ERBB2-amplified breast carcinomas enhances ErbB-2 oncogenic potency and favors resistance to Herceptin. *Oncogene.* 24:4540–4548. doi:10.1038/sj.onc.1208658

Anastasi, S., M.F. Baietti, Y. Frosi, S. Alemà, and O. Segatto. 2007. The evolutionarily conserved EBR module of RALT/MIG6 mediates suppression of the EGFR catalytic activity. *Oncogene.* 26:7833–7846. doi:10.1038/sj.onc.1210590

Ballarò, C., S. Ceccarelli, C. Tiveron, L. Tatangelo, A.M. Salvatore, O. Segatto, and S. Alemà. 2005. Targeted expression of RALT in mouse skin inhibits epidermal growth factor receptor signalling and generates a Waved-like phenotype. *EMBO Rep.* 6:755–761. doi:10.1038/sj.embor.7400458

Burgess, A.W., H.S. Cho, C. Eigenbrot, K.M. Ferguson, T.P. Garrett, D.J. Leahy, M.A. Lemmon, M.X. Sliwkowski, C.W. Ward, and S. Yokoyama. 2003. An open-and-shut case? Recent insights into the activation of EGF/ErbB receptors. *Mol. Cell.* 12:541–552. doi:10.1016/S1097-2765(03)00350-2

Cai, J., F.F. Yi, L. Yang, D.F. Shen, Q. Yang, A. Li, A.K. Ghosh, Z.Y. Bian, L. Yan, Q.Z. Tang, et al. 2009. Targeted expression of receptor-associated late transducer inhibits maladaptive hypertrophy via blocking epidermal growth factor receptor signaling. *Hypertension.* 53:539–548. doi:10.1161/HYPERTENSIONAHA.108.120816

Chen, W.S., C.S. Lazar, K.A. Lund, J.B. Welsh, C.P. Chang, G.M. Walton, C.J. Der, H.S. Wiley, G.N. Gill, and M.G. Rosenfeld. 1989. Functional independence of the epidermal growth factor receptor from a domain required for ligand-induced internalization and calcium regulation. *Cell.* 59:33–43. doi:10.1016/0092-8674(89)90867-2

Ferby, I., M. Reschke, O. Kudlacek, P. Knyazev, G. Pantè, K. Amann, W. Sommergruber, N. Kraut, A. Ullrich, R. Fässler, and R. Klein. 2006. Mig6 is a negative regulator of EGF receptor-mediated skin morphogenesis and tumor formation. *Nat. Med.* 12:568–573. doi:10.1038/nm1401

Fiorentino, L., C. Pertica, M. Fiorini, C. Talora, M. Crescenzi, L. Castellani, S. Alemà, P. Benedetti, and O. Segatto. 2000. Inhibition of ErbB-2 mitogenic and transforming activity by RALT, a mitogen-induced signal transducer which binds to the ErbB-2 kinase domain. *Mol. Cell. Biol.* 20:7735–7750. doi:10.1128/MCB.20.20.7735-7750.2000

Fry, W.H., L. Kotelawala, C. Sweeney, and K.L. Carraway III. 2009. Mechanisms of ErbB receptor negative regulation and relevance in cancer. *Exp. Cell Res.* 315:697–706. doi:10.1016/j.yexcr.2008.07.022

Hackel, P.O., M. Gishizky, and A. Ullrich. 2001. Mig-6 is a negative regulator of the epidermal growth factor receptor signal. *Biol. Chem.* 382:1649–1662. doi:10.1515/BC.2001.200

Haglund, K., S. Sigismund, S. Polo, I. Szymkiewicz, P.P. Di Fiore, and I. Dikic. 2003. Multiple monoubiquitination of RTKs is sufficient for their endocytosis and degradation. *Nat. Cell Biol.* 5:461–466. doi:10.1038/ncb983

Hislop, J.N., A. Marley, and M. Von Zastrow. 2004. Role of mammalian vacuolar protein-sorting proteins in endocytic trafficking of a non-ubiquitinated G protein-coupled receptor to lysosomes. *J. Biol. Chem.* 279:22522–22531. doi:10.1074/jbc.M311062200

Huang, F., and A. Sorkin. 2005. Growth factor receptor binding protein 2-mediated recruitment of the RING domain of Cbl to the epidermal growth factor receptor is essential and sufficient to support receptor endocytosis. *Mol. Biol. Cell.* 16:1268–1281. doi:10.1091/mbc.E04-09-0832

Hussain, N.K., S. Jenna, M. Glogauer, C.C. Quinn, S. Wasiak, M. Guipponi, S.E. Antonarakis, B.K. Kay, T.P. Stossel, N. Lamarche-Vane, and P.S. McPherson. 2001. Endocytic protein intersectin-l regulates actin assembly via Cdc42 and N-WASP. *Nat. Cell Biol.* 3:927–932. doi:10.1038/ncb1001-927

Jiang, X., F. Huang, A. Marusyk, and A. Sorkin. 2003. Grb2 regulates internalization of EGF receptors through clathrin-coated pits. *Mol. Biol. Cell.* 14:858–870. doi:10.1091/mbc.E02-08-0532

Johannessen, L.E., N.M. Pedersen, K.W. Pedersen, I.H. Madshus, and E. Stang. 2006. Activation of the epidermal growth factor (EGF) receptor induces formation of EGF receptor- and Grb2-containing clathrin-coated pits. *Mol. Cell. Biol.* 26:389–401. doi:10.1128/MCB.26.2.389-401.2006

Lenferink, A.E., R. Pinkas-Kramarski, M.L. van de Poll, M.J. van Vugt, L.N. Klapper, E. Tzahar, H. Waterman, M. Sela, E.J. van Zoelen, and Y. Yarden. 1998. Differential endocytic routing of homo- and hetero-dimeric ErbB tyrosine kinases confers signaling superiority to receptor heterodimers. *EMBO J.* 17:3385–3397. doi:10.1093/emboj/17.12.3385

Levkowitz, G., H. Waterman, E. Zamir, Z. Kam, S. Oved, W.Y. Langdon, L. Beguinot, B. Geiger, and Y. Yarden. 1998. c-Cbl/Sli-1 regulates endocytic sorting and ubiquitination of the epidermal growth factor receptor. *Genes Dev.* 12:3663–3674. doi:10.1101/gad.12.23.3663

Levkowitz, G., H. Waterman, S.A. Ettenberg, M. Katz, A.Y. Tsygankov, I. Alroy, S. Lavi, K. Iwai, Y. Reiss, A. Ciechanover, et al. 1999. Ubiquitin ligase activity and tyrosine phosphorylation underlie suppression of growth factor signaling by c-Cbl/Sli-1. *Mol. Cell.* 4:1029–1040. doi:10.1016/S1097-2765(00)80231-2

Loerke, D., M. Mettlen, D. Yarar, K. Jaqaman, H. Jaqaman, G. Danuser, and S.L. Schmid. 2009. Cargo and dynamin regulate clathrin-coated pit maturation. *PLoS Biol.* 7:e57. doi:10.1371/journal.pbio.1000057

Macia, E., M. Ehrlich, R. Massol, E. Boucrot, C. Brunner, and T. Kirchhausen. 2006. Dynasore, a cell-permeable inhibitor of dynamin. *Dev. Cell.* 10:839–850. doi:10.1016/j.devcel.2006.04.002

Marmor, M.D., and Y. Yarden. 2004. Role of protein ubiquitylation in regulating endocytosis of receptor tyrosine kinases. *Oncogene.* 23:2057–2070. doi:10.1038/sj.onc.1207390

Martin, N.P., R.P. Mohney, S. Dunn, M. Das, E. Scappini, and J.P. O'Bryan. 2006. Intersectin regulates epidermal growth factor receptor endocytosis, ubiquitylation, and signaling. *Mol. Pharmacol.* 70:1643–1653. doi:10.1124/mol.106.028274

Mayer, B.J. 2001. SH3 domains: complexity in moderation. *J. Cell Sci.* 114:1253–1263.

McGavin, M.K., K. Badour, L.A. Hardy, T.J. Kubiseski, J. Zhang, and K.A. Siminovitch. 2001. The intersectin 2 adaptor links Wiskott Aldrich Syndrome protein (WASp)-mediated actin polymerization to T cell antigen receptor endocytosis. *J. Exp. Med.* 194:1777–1787. doi:10.1084/jem.194.12.1777

Mettlen, M., M. Stoeber, D. Loerke, C.N. Antonescu, G. Danuser, and S.L. Schmid. 2009. Endocytic accessory proteins are functionally distinguished by their differential effects on the maturation of clathrin-coated pits. *Mol. Biol. Cell.* 20:3251–3260. doi:10.1091/mbc.E09-03-0256

Mosesson, Y., G.B. Mills, and Y. Yarden. 2008. Derailed endocytosis: an emerging feature of cancer. *Nat. Rev. Cancer.* 8:835–850. doi:10.1038/nrc2521

Nikolaienko, O., I. Skrypkina, L. Tsyba, Y. Fedyshyn, D. Morderer, V. Buchman, S. de la Luna, L. Drobot, and A. Rynditch. 2009. Intersectin 1 forms a complex with adaptor protein Ruk/CIN85 in vivo independently of epidermal growth factor stimulation. *Cell. Signal.* 21:753–759. doi:10.1016/j.cellsig.2009.01.013

O'Bryan, J.P., R.P. Mohney, and C.E. Oldham. 2001. Mitogenesis and endocytosis: What's at the INTERSECTIoN? *Oncogene.* 20:6300–6308. doi:10.1038/sj.onc.1204773

Orth, J.D., and M.A. McNiven. 2006. Get off my back! Rapid receptor internalization through circular dorsal ruffles. *Cancer Res.* 66:11094–11096. doi:10.1158/0008-5472.CAN-06-3397

Praefcke, G.J., M.G. Ford, E.M. Schmid, L.E. Olesen, J.L. Gallop, S.Y. Peak-Chew, Y. Vallis, M.M. Babu, I.G. Mills, and H.T. McMahon. 2004. Evolving nature of the AP2 alpha-appendage hub during clathrin-coated vesicle endocytosis. *EMBO J.* 23:4371–4383. doi:10.1038/sj.emboj.7600445

Pruss, R.M., H.R. Herschman, and V. Klement. 1978. 3T3 variants lacking receptors for epidermal growth factor are susceptible to transformation by Kirsten sarcoma virus. *Nature.* 274:272–274. doi:10.1038/274272a0

Pucharcos, C., C. Casas, M. Nadal, X. Estivill, and S. de la Luna. 2001. The human intersectin genes and their spliced variants are differentially expressed. *Biochim. Biophys. Acta.* 1521:1–11.

Reschke, M., I. Ferby, E. Stepniak, N. Seitzer, D. Horst, E.F. Wagner, and A. Ullrich. 2009. Mitogen-inducible gene-6 is a negative regulator of epidermal growth factor receptor signaling in hepatocytes and human hepatocellular carcinoma. *Hepatology.* 51:1383–1390.

Schmid, E.M., M.G. Ford, A. Burtey, G.J. Praefcke, S.Y. Peak-Chew, I.G. Mills, A. Benmerah, and H.T. McMahon. 2006. Role of the AP2 beta-appendage hub in recruiting partners for clathrin-coated vesicle assembly. *PLoS Biol.* 4:e262. doi:10.1371/journal.pbio.0040262

Sengar, A.S., W. Wang, J. Bishay, S. Cohen, and S.E. Egan. 1999. The EH and SH3 domain Ese proteins regulate endocytosis by linking to dynamin and Eps15. *EMBO J.* 18:1159–1171. doi:10.1093/emboj/18.5.1159

Sibilia, M., R. Kroismayr, B.M. Lichtenberger, A. Natarajan, M. Hecking, and M. Holcmann. 2007. The epidermal growth factor receptor: from development to tumorigenesis. *Differentiation.* 75:770–787. doi:10.1111/j.1432-0436.2007.00238.x

Sigismund, S., E. Argenzio, D. Tosoni, E. Cavallaro, S. Polo, and P.P. Di Fiore. 2008. Clathrin-mediated internalization is essential for sustained EGFR signaling but dispensable for degradation. *Dev. Cell.* 15:209–219. doi:10.1016/j.devcel.2008.06.012

Simpson, F., N.K. Hussain, B. Qualmann, R.B. Kelly, B.K. Kay, P.S. McPherson, and S.L. Schmid. 1999. SH3-domain-containing proteins function at distinct steps in clathrin-coated vesicle formation. *Nat. Cell Biol.* 1:119–124. doi:10.1038/10091

Sorkin, A., and L.K. Goh. 2009. Endocytosis and intracellular trafficking of ErbBs. *Exp. Cell Res.* 315:683–696. doi:10.1016/j.yexcr.2008.07.029

Sorkin, A., K. Helin, C.M. Waters, G. Carpenter, and L. Beguinot. 1992. Multiple autophosphorylation sites of the epidermal growth factor receptor are

essential for receptor kinase activity and internalization. Contrasting significance of tyrosine 992 in the native and truncated receptors. *J. Biol. Chem.* 267:8672–8678.

Sorkina, T., F. Huang, L. Beguinot, and A. Sorkin. 2002. Effect of tyrosine kinase inhibitors on clathrin-coated pit recruitment and internalization of epidermal growth factor receptor. *J. Biol. Chem.* 277:27433–27441. doi:10.1074/jbc.M201595200

Traub, L.M. 2009. Tickets to ride: selecting cargo for clathrin-regulated internalization. *Nat. Rev. Mol. Cell Biol.* 10:583–596. doi:10.1038/nrm2751

Xu, D., A. Makkinje, and J.M. Kyriakis. 2005. Gene 33 is an endogenous inhibitor of epidermal growth factor (EGF) receptor signaling and mediates dexamethasone-induced suppression of EGF function. *J. Biol. Chem.* 280:2924–2933. doi:10.1074/jbc.M408907200

Yamabhai, M., N.G. Hoffman, N.L. Hardison, P.S. McPherson, L. Castagnoli, G. Cesareni, and B.K. Kay. 1998. Intersectin, a novel adaptor protein with two Eps15 homology and five Src homology 3 domains. *J. Biol. Chem.* 273:31401–31407. doi:10.1074/jbc.273.47.31401

Zhang, X., J. Gureasko, K. Shen, P.A. Cole, and J. Kuriyan. 2006. An allosteric mechanism for activation of the kinase domain of epidermal growth factor receptor. *Cell.* 125:1137–1149. doi:10.1016/j.cell.2006.05.013

Zhang, X., K.A. Pickin, R. Bose, N. Jura, P.A. Cole, and J. Kuriyan. 2007. Inhibition of the EGF receptor by binding of MIG6 to an activating kinase domain interface. *Nature.* 450:741–744. doi:10.1038/nature05998

Zhang, Y.W., B. Staal, Y. Su, P. Swiatek, P. Zhao, B. Cao, J. Resau, R. Sigler, R. Bronson, and G.F. Vande Woude. 2007. Evidence that MIG-6 is a tumor-suppressor gene. *Oncogene.* 26:269–276. doi:10.1038/sj.onc.1209790